1. Supplemental Methods.

ROI Identification. Regions of Interest (ROIs) were identified offline by three methods. The first, which was the principal method used for the dataset, was human operator driven identification based upon both the high-resolution reference image and repeated playing of the time-series movie. Two additional methods were used to verify the results of this hand-mapping procedure. Correlation maps were generated by choosing very small localised "seed" areas of pixels, taking the average of their intensity at each frame, and generating an image of the correlation of that time series which each spatial location. The last method involved the application of a customized spatial independent component analysis (sICA) procedure to extract ROIs corresponding to minimally inter-dependent spatial regions of pixels, based on the method described in reference (Reidl et al., 2007). This third method was applied systematically to the entire dataset, verifying the accuracy of the ROI choices made by method 1 in the parameter regimes in which it was applicable, and in a few cases allowing small human operator errors to be corrected. All three methods result in pixel clusters lining up in a narrow rostrocaudal plane (Fig. S1). These three methods were implemented as follows:

(i) Human operator ROI selection. This method was the principal method used to analyze the dataset. Based upon both the high-resolution reference image and repeated playing of the time-series movie, pixels were marked out as belonging to a region using a custom-written graphical user interface, if they satisfied the following criteria: (a) they underwent high amplitude, temporally asymmetric (calcium transient like) fluctuations, (b) they underwent such fluctuations at the same time as other pixels in the region, (c) on no occasion did they undergo such large amplitude fluctuations when the other pixels in the region did not. It is important to reiterate that it was not possible to select ROIs simply by looking at a static reference image; time-series information was extremely important in order to delineate the pixels satisfying the above criteria.

(ii) Correlation maps. For each desired region, a small seed was chosen (see Figure 6A), and a time-series extracted by averaging the values of all pixels within the seed region for each frame. This was then cross-correlated with all pixel time series to form an image (Fig. 6B). To obtain relatively smooth (and thus less vulnerable to movement artifact) ROIs, the image was convolved with an anisotropic gaussian filter (elongated 2.7:1 in the direction of the dendrites) and thresholded to retain a fixed percentage of pixels in the mask (2.75% both typically and in the example of Figure S1).

(iii) sICA analysis was performed along similar lines to (Reidl et al., 2007), with the exception that the FastICA algorithm was used (Bingham and Hyvärinen, 2000) in order to improve computational efficiency. Briefly, data (spatiotemporal movies) were

preprocessed using principal component analysis (PCA) in order to reduce dimensionality, retaining 20 principal components. Spatial images representing each component were squared, filtered and thresholded in order to extract individual ROIs. It is possible to directly extract a time-series associated with each component, however, we found that in practice a more useful time-series for the purpose of examining spatially localized fluorescence signals was obtained from the ROI masks.

We compared methods (ii) and (iii) on a few selected examples, and found them to perform quite similarly, although method (ii) required more human operator time. We compared methods (i) and (iii) across the entire dataset. Our conclusion was that human operator ROI selection was the most flexible approach, in that ROIs could be obtained under a wider range of circumstances (e.g. at a lower zoom so that a greater area could be imaged), but that it was by far the most time consuming method. If the area imaged was not too large (exact area depending on labeling quality, but of the order of 100 x 100 microns), it was practical to use sICA as a largely automated ROI selection procedure; if the area was too large, or signal strength poor, then regions would be missed that may be identifiable by eye. We found that the best results were achieved by using an sICA run as a guide for human operator selection of regions of interest. For the dataset described in this paper, we initially carried out ROI selection for the entire dataset by hand, and subsequently used sICA to examine each imaging run, and in some few cases to correct human errors.

Analysis of Time Series Data. Fluorescence time-series corresponding to the average intensity of all pixels within an ROI, in each frame, were extracted. Note that, depending upon the vertical extent of the structure imaged, the pixels will not have been acquired at precisely the same time, as acquisition occurs by frame scan. For the present analysis, this is not taken into consideration: all such pixels were averaged together, with the frame rate defining the temporal precision of measurement (Aertsen et al., 1989).

The amplitude of measured calcium transients varies from event to event (primarily due to aliasing). To provide a quantitative index of the strength of observed sensory responses, we estimated the signal-to-noise ratio pertaining to fluorescence measurement of the sensory response of each dendritic ROI as

$$SNR = \frac{(\Delta F)^2}{\sigma_{\Delta F}^2} \tag{1}$$

where ΔF is the average change in evoked fluorescence, measured in comparison to the three time-bins prior to stimulus delivery, and $\sigma_{\Delta F}$ is the standard deviation of the evoked change in fluorescence across trials. This quantity incorporates both shot noise and trial-to-trial variability into its noise definition, and is bounded from above by the true signal-to-noise ratio of CS sensory responses.

To obtain a measure of the correlation between signals in each ROI, each time series was smoothed with a median filter (for frame durations <128 ms only) and the rectified derivative obtained. The cross-covariance of these rectified derivative signals was then obtained as a function of time lag, and scaled to normalize the auto-covariance at zero time lag (i.e., to normalize for signal power). Cross-covariance computed directly from mean-subtracted fluorescence time series yielded very similar results, but with lower signal-to-noise ratio. A 90% confidence interval for the covariance that might be expected by chance was obtained by spike detection, followed by the scrambling of spike times and the generation of surrogate data by convolution with a template corresponding to the average calcium transient.

Calcium transient event detection. We used a template detection procedure to detect events for analyses (such as inter-event statistics) which could not readily be carried out upon the fluorescence signal directly. The algorithm is similar to those used for detecting action potentials in extracellular recordings (Wörgötter et al., 1986;Bergman and DeLong, 1992) and for detecting spontaneous synaptic events (Clements and Bekkers, 1997). Our template detection algorithm is applied to each time-series trace, separately for each ROI:

1. Select from the time series 10 template candidates that exhibit most clear calcium transient characteristics, defined as (i) a positive first derivative followed by (ii) a long decay, with (iii) an exponential shape, with positive second derivative. These candidates are averaged and used to form the template.
2. Compute the inner product of the template with the portion of the trace underlying it, sliding the template along the trace. Remove values below the median and raise to the power of two. This forms the template match signal.
3. Form a spike train by thresholding the template match signal.
4. Convolve the spike train with the template; return to step3, adjusting threshold, until the correlation coefficient between the convolved spike train and the original fluorescence signal is maximised.

Performance of the algorithm on four cells, from which electrophysiological recordings were made simultaneous with fluorescence measurement, are shown in Fig. S3. Event detections were considered to be correct only if they matched an action potential that had not already been allocated to a detected event, following Greenberg et al (Greenberg et al., 2008).

JPSTH Analysis. The Joint Post-Stimulus Time Histogram (JPSTH) (Aertsen et al., 1989) was computed directly from the fluorescence time series. Following Aertsen et al, we computed the normalized JPSTH as

$$nJPSTH = \frac{\langle \phi_1 \phi_2 \rangle - \langle \phi_1 \rangle \langle \phi_2 \rangle}{\sigma_{\phi_1} \sigma_{\phi_2}} \qquad (2)$$

where ϕ_i is the relative change of fluorescence of cell *i* from the local (trial) average, $\phi_i = (F_i - \overline{F_i})$, and $\langle . \rangle$ indicates the average (expectation) across trials. This procedure thus corrects for synchrony due to the fact that a pair of cells may fire at the same time due to the fact that they are responding to the same stimulus, by subtracting the predictor provided by the product of the marginals (PSTHs). The nJPSTH is finally scaled by normalizing for the standard deviation across trials of the predictor, resulting in a quantity analogous to the Pearson correlation coefficient. In order to average data recorded at different frame rates, individual JPSTH results were interpolated with a cubic spline function. As the methods for significance criteria used by Aertsen et al (Palm et al., 1988) rely upon results valid only for discrete counts, we instead used a one-sample t-test to test the hypothesis that the mean of the distribution of single trial nJPSTH values significantly exceeded zero. Although the distributions of nJPSTH values were found not to be Gaussian, the t-test is conservative for long-tailed distributions (Benjamini, 1983).

References

Aertsen AM, Gerstein GL, Habib MK, Palm G (1989) Dynamics of neuronal firing correlation: modulation of "effective connectivity". J Neurophysiol 61:900-917.

Benjamini Y (1983) Is the t-test really conservative when the parent distribution is long-tailed? J Am Stat Assoc 78:645-654.

Bergman H, DeLong MR (1992) A personal computer-based spike detector and sorter: implementation and evaluation. J Neurosci Methods 41:187-197.

Bingham E, Hyvärinen A (2000) A fast fixed-point algorithm for independent component analysis of complex valued signals. Int J Neural Syst 10:1-8.

Clements JD, Bekkers JM (1997) Detection of spontaneous synaptic events with an optimally scaled template. Biophys J 73:220-229.

Greenberg DS, Houweling AR, Kerr JN (2008) Population imaging of ongoing neuronal activity in the visual cortex of awake rats. Nat Neurosci.

Palm G, Aertsen AM, Gerstein GL (1988) On the significance of correlations among neuronal spike trains. Biol Cybern 59:1-11.

Reidl J, Starke J, Omer DB, Grinvald A, Spors H (2007) Independent component analysis of high-resolution imaging data identifies distinct functional domains. Neuroimage 34:94-108.

Schultz SR, Panzeri S (2001) Temporal correlations and neural spike train entropy. Phys Rev Lett 86:5823-5826.

Wörgötter F, Daunicht WJ, Eckmiller R (1986) An on-line spike form discriminator for extracellular recordings based on an analog correlation technique. J Neurosci Methods 17:141-151.

Fig. S1 Different ROI identification procedures result in similar regions and time series. **A** A 127 micron square region stained with Oregon Green BAPTA-1 AM. A small region of dendrites has been marked out (green overlay) as a seed region for correlation analysis. Scale bar, 25 μm. **B** Map of the mean-subtracted cross-correlation of the times-series associated with each pixel. **C** Six ROIs defined by choosing seeds at different places in the image by hand, and smoothing and thresholding the resulting correlation maps. **D** The independent spatial component extracted by the sICA procedure (see text) for the same dendrite as described in *B*. **E** Six regions obtained from sICA components by smoothing and thresholding with identical parameters to *C*. **F** ROIs obtained by the human operator by hand, using information from the average spatial image *(A)* and the spatiotemporal movie. **G** Comparison of the time-series (3-point median filtered) extracted via the sICA (i) and hand-selection (ii) methods, for the three regions of *E* indicated by the color code. The time-series differ in minor details, but are very close in overall structure – with normalized cross-covariance between (i) and (ii) ranging from 0.89 to 0.92. Scale identical across all panels.

Fig. S2 As a method for measuring the relative event rates in spontaneous and evoked conditions, which did not depend upon a template-matching event-detection algorithm, we directly measured fluctuations in the fluorescence signal. We integrated the positive-going fluctuations (rectified derivative) in the relative fluorescence signals over the sensory-evoked / spontaneous period (which includes many airpuff cycles), and divided by the duration, thus yielding a measure which can be thought of as ΔF/Fs per second. Sensory-evoked calcium transients were found not to occur at rates significantly exceeding the spontaneous rate (Kolmogorov-Smirnov test, n=130, p=0.45), as shown in Fig. 3C, despite clear sensory-locked responses being visible in the PSTH. This was equally true after the administration of harmaline (n=46, p=0.56).

Fig. S3 Analysis of performance of the event-detection algorithm, using simultaneous electrophysiology and calcium imaging. **A, B** Example traces showing relative change in fluorescence traces (top), together with the template-match signal (see SI Text, magenta trace). The electrophysiologically measured spike train is shown below in blue, and the detected event train in green. **C** The fraction of correct detections (top traces) and false positives (bottom traces) as a function of the temporal precision used to determine whether a deteced event matched a true event. Event detections were considered to be correct only if they matched an action potential that had not already been allocated to a detected event. Individual traces from different regions (n=4) shown in grey, mean shown by thick black line. Lines begin at the frame sampling duration, 147 ms in each of these cases. **D** Receiver operating characteristic (ROC) analysis for a temporal precision of 0.22 sec. Blue circles indicate the fraction of correct detections and false positives

with the event detection threshold at the setting which maximized the correlation between the actual fluorescence trace and the event train convolved with the template for that cell.

Fig. S4 The additional amount of synchrony revealed by the nJPSTH does not depend upon the strength of sensory responses. The ordinate shows the difference between the peak nJPSTH value in the period 0.0 to 0.4 sec after stimulus onset, and the nJPSTH prior to stimulus onset (average from 0.2 to 0.4 sec prior). The co-ordinate shows the geometric mean of the average relative change in fluorescence (i.e. trial-averaged response magnitude) from each cell in the pair. No statistically significant relationship between these quantities was evident (correlation coefficient 0.08, not significant at $p=0.10$; $n=123$ pairs with SNR exceeding 0.2).

Fig. S5 With the information estimation strategy that we adopted, the number of trials per stimulus available provided adequate sampling performance. The figure shows CS spatial pattern and count information (as a fraction of their asymptotic value) for Poisson surrogate data generated with up to 5000 trials per stimulus (7 cells, PSTH as for the example in Fig. 5A). This procedure has previously been found to be an effective way to estimate the size of residual finite sampling bias (Schultz and Panzeri, 2001). At 200 trials per stimulus, residual bias in the pattern code is estimated to be 5%, which is substantially smaller than the size of the effects that we see.

Fig. S6 Comparison of signal detection and signal timing information for each ensemble. Do the results for information about stimulus timing hold also for signal detection? Indeed, the stimulus timing information calculation can be viewed as a generalization of a signal detection information calculation – in both cases, the "stimuli" are the times from which each response bin is drawn; in the latter case, we simply draw two response bins, one from a time prior to stimulus onset (noise only) and one from the time of the peak sensory-evoked response (signal plus noise). In principle, the signal detection information might be either higher or lower than the timing information. This figure shows two things: firstly, that the signal detection information correlates strongly with the timing information; secondly, that, when viewed at the temporal resolution of the current calcium imaging experiment, signal detection information is slightly more reliable than signal timing information. The latter point might be expected to be a limitation of the temporal resolution of the recording approach used, and it would be useful to revisit this issue with a higher temporal resolution imaging approach.

Fig. S7 Our results are conservative with regard to both event misses and false positives, as both tend to reduce correlation and thus reduce spike pattern information more than spike count information. The figure shows, for the example of Fig. 5A, the effect of deleting 20% of spikes or of inserting 10% additional spikes.

2. Supplemental Movie 1

Maximum intensity projection of a three-dimensional image stack (Fig 1A), rotating about the vertical axis.

3. Supplemental Movie 2

Maximum intensity projection of a three-dimensional image stack (Fig 1B), rotating about the vertical axis.

4. Supplemental Movie 3

A typical time-series movie of fluorescence intensity. Individual frames were of 73.6 ms duration and 256x32 pixel resolution. The change in fluorescence has been overlaid on the average fluorescence for viewing. Spatial width of region: 127 μm.

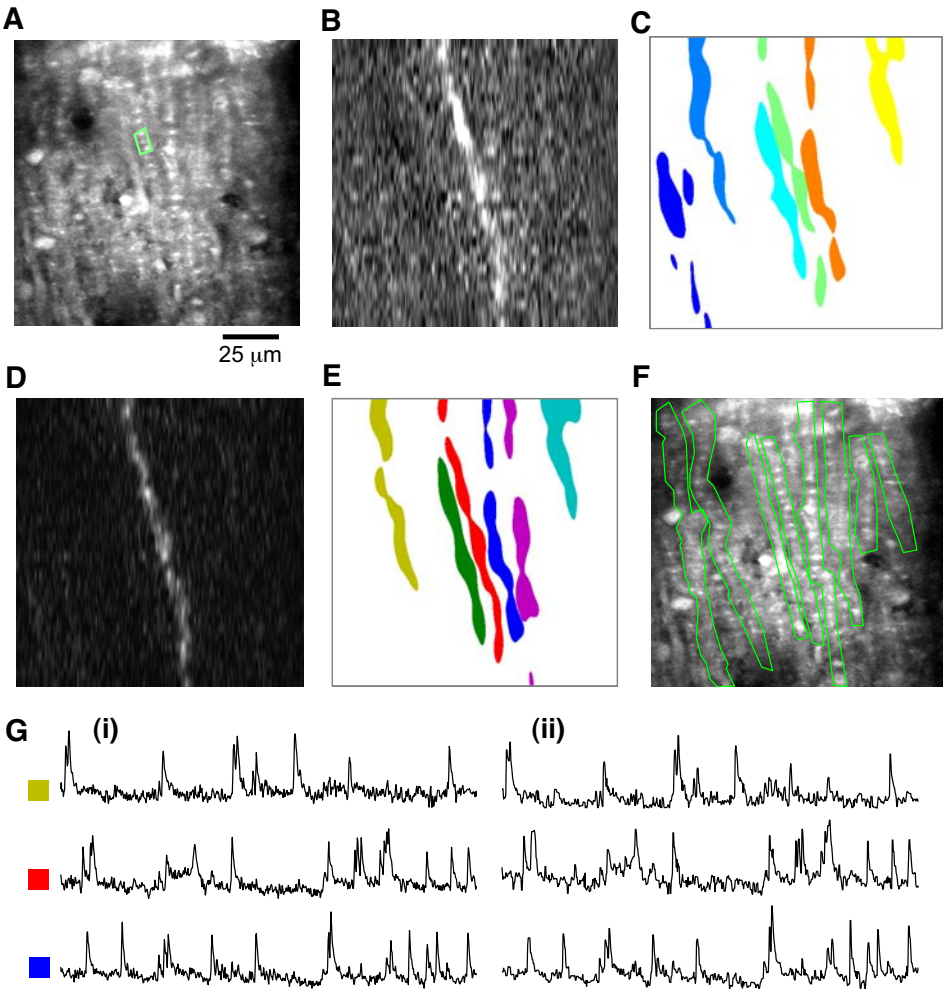

Figure S1

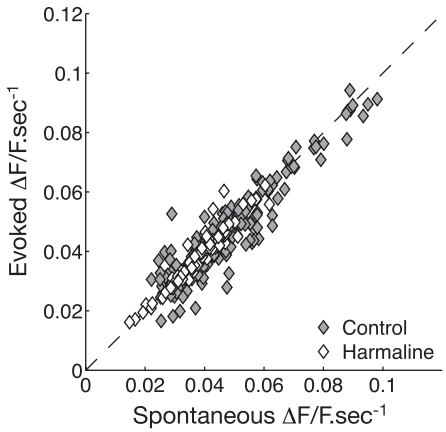
0.12
0.1
0.08
0.06
0.04
0.02
0
Evoked ΔF/F.sec-1
0
0.02
0.04
0.06
0.08
0.1
Spontaneous ΔF/F.sec-1
Control
Harmaline

Figure S2

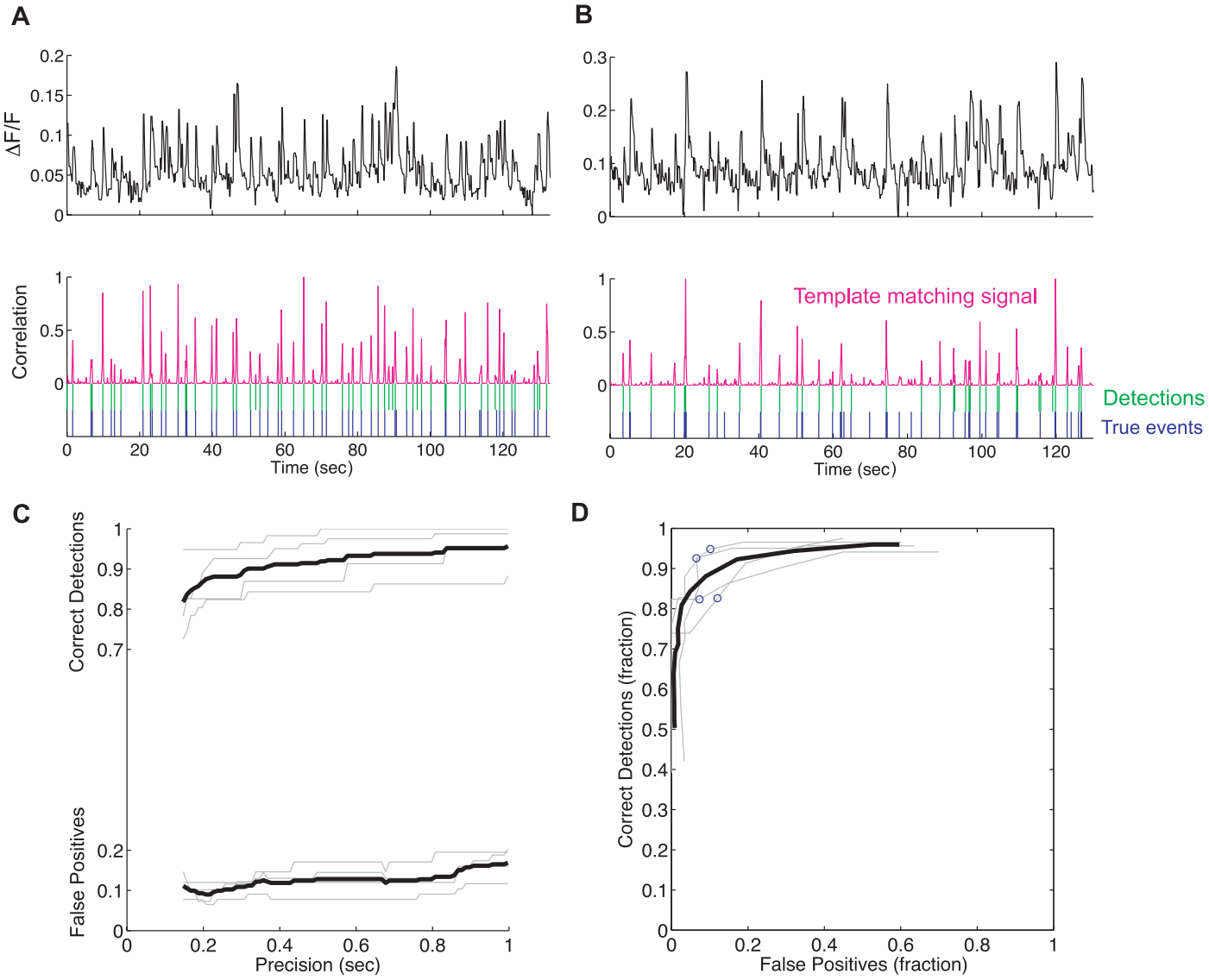
A
B
ΔF/F
Correlation
Time (sec)
Template matching signal
Detections
True events
C
Correct Detections
False Positives
Precision (sec)
D
Correct Detections (fraction)
False Positives (fraction)

Figure S3

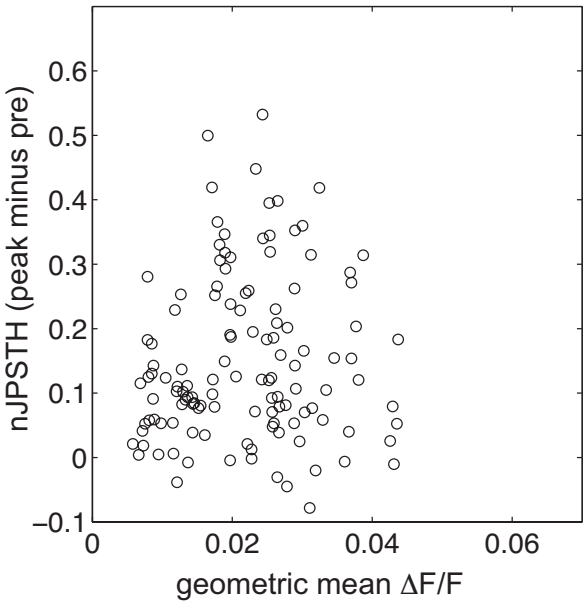
nJPSTH (peak minus pre)
0.6
0.5
0.4
0.3
0.2
0.1
0
−0.1
0
0.02
0.04
0.06
geometric mean ΔF/F

Figure S4

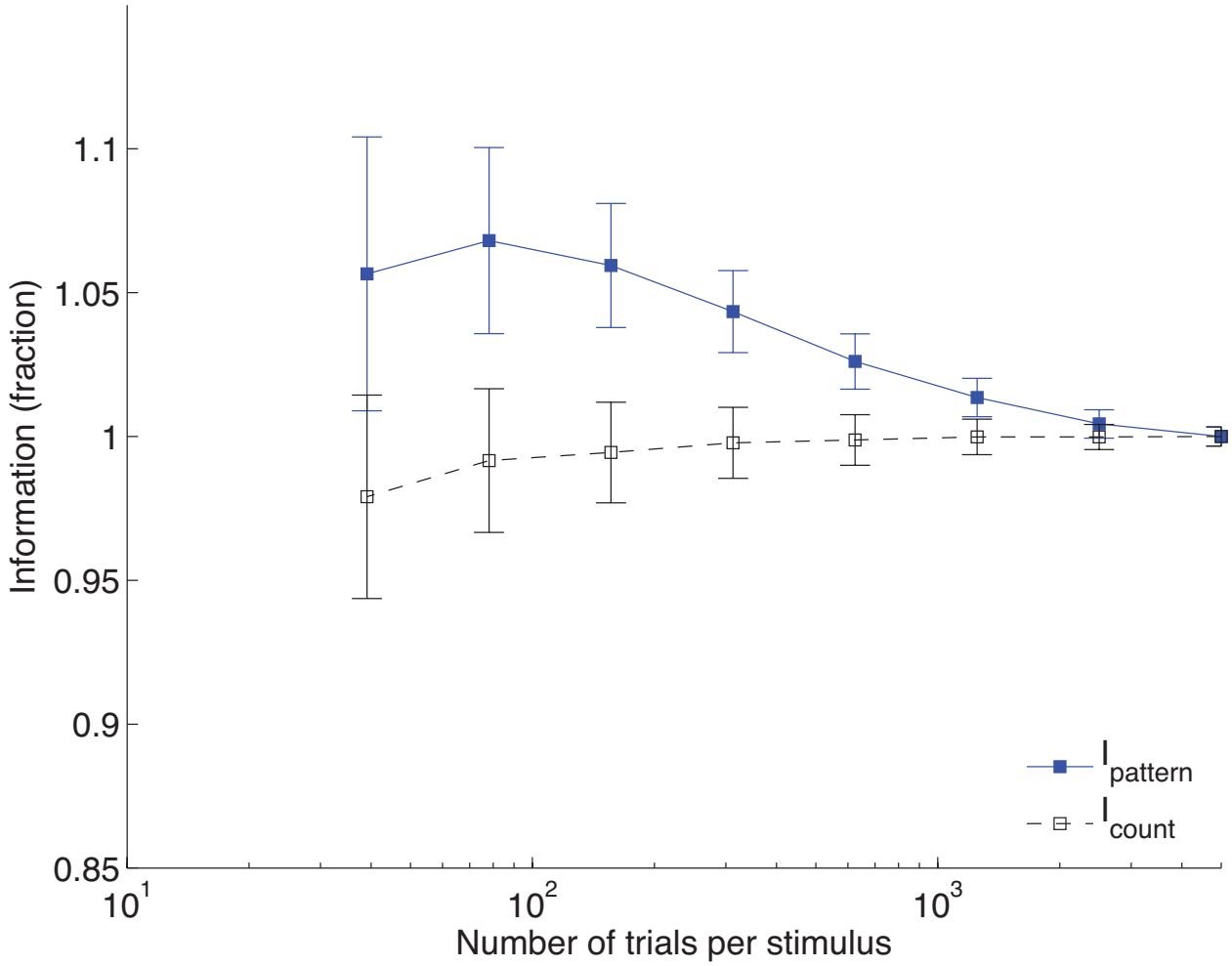
1.1
1.05
1
0.95
0.9
0.85
Information (fraction)
10^1
10^2
10^3
Number of trials per stimulus
$I_{pattern}$
I_{count}

Figure S5

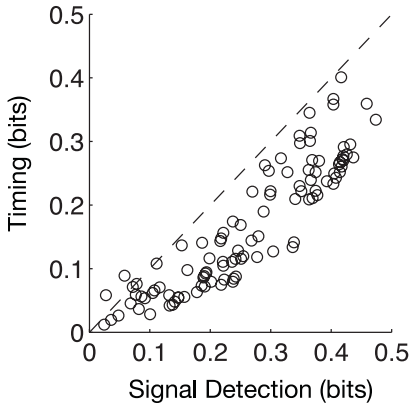
0.5
0.4
0.3
0.2
0.1
0
Timing (bits)
0
0.1
0.2
0.3
0.4
0.5
Signal Detection (bits)

Figure S6

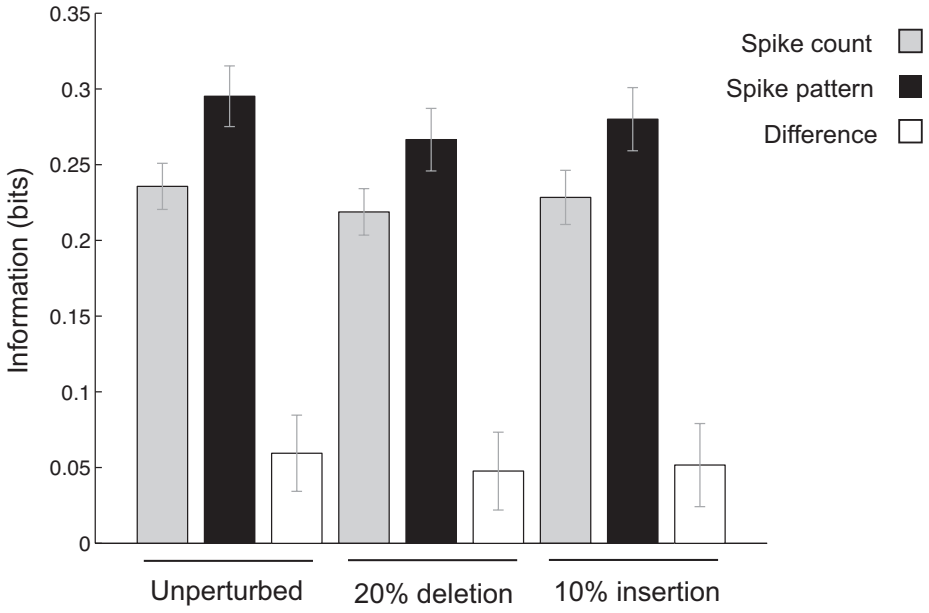
0.35
0.3
0.25
0.2
0.15
0.1
0.05
0
Information (bits)
Spike count
Spike pattern
Difference
Unperturbed
20% deletion
10% insertion

Figure S7